Towards a Mg Lattice Clock: Observation of the $^1S_0$-$^3P_0$ Transition and Determination of the Magic Wavelength

A. P. Kulosa,[1] D. Fim,[1] K. H. Zipfel,[1] S. Rühmann,[1] S. Sauer,[1] N. Jha,[1] K. Gibble,[1,2] W. Ertmer,[1] E. M. Rasel,[1] M. S. Safronova,[3,4] U. I. Safronova,[5] and S. G. Porsev[3,6]

[1]*Institut für Quantenoptik, Leibniz Universität Hannover, Welfengarten 1, 30167 Hannover, Germany*
[2]*Department of Physics, The Pennsylvania State University, University Park, Pennsylvania 16802, USA*
[3]*Department of Physics and Astronomy, University of Delaware, Newark, Delaware 19716, USA*
[4]*Joint Quantum Institute, NIST and the University of Maryland, College Park, Maryland 20899, USA*
[5]*Department of Physics, University of Nevada, Reno, Nevada 89557, USA*
[6]*Petersburg Nuclear Physics Institute, Gatchina 188300, Russia*

(Received 5 August 2015; published 9 December 2015)

We optically excite the electronic state $3s3p\ ^3P_0$ in ^{24}Mg atoms, laser cooled and trapped in a magic-wavelength lattice. An applied magnetic field enhances the coupling of the light to the otherwise strictly forbidden transition. We determine the magic wavelength, the quadratic magnetic Zeeman shift, and the transition frequency to be 468.46(21) nm, $-206.6(2.0)$ MHz/T^2, and 655 058 646 691(101) kHz, respectively. These are compared with theoretical predictions and results from complementary experiments. We also develop a high-precision relativistic structure model for magnesium, give an improved theoretical value for the blackbody radiation shift, and discuss a clock based on bosonic magnesium.

DOI: 10.1103/PhysRevLett.115.240801 PACS numbers: 06.30.Ft, 31.15.ac, 37.10.Jk, 42.62.Fi

The frequencies of optical clocks are currently measured with a fractional accuracy and precision of nearly 10^{-18} [1–4]. A potentially limiting systematic frequency shift of both ion and optical lattice clocks is the ac Stark shift from room-temperature blackbody radiation (BBR) [5,6]. Clock transitions with small BBR sensitivities are an attractive approach to even higher accuracies. Among these are neutral Hg and Mg, In^+, and especially the Al^+ ion clock transition, which all have significantly smaller BBR sensitivities than Sr and Yb lattice clocks and Cs microwave clocks.

In this Letter, we report the spectroscopy of the Mg clock transition in a magic-wavelength optical lattice, which gives equal ac Stark shifts of the clock states. We measure the transition frequency [7,8] and its magic wavelength and quadratic Zeeman shift, which were recently predicted [9–12].

Along with our measurements, we developed a more refined atomic structure model to calculate both the magic wavelength as well as the static BBR shift. For less massive atoms, such as Mg, these models are more accurate than for heavier elements like Sr and Yb, and spectroscopy of low-mass elements generally represents an interesting test bed for validating improved theoretical models [13]. Both our theoretical and experimental results for the magic wavelength agree at a level of better than 1% and restrict the value, which was estimated to fall between 466 and 480 nm [9–11]. Our model for Mg predicts a static BBR shift to be 8 and 5 times lower than those measured for Sr and Yb, respectively [14,15]. Apart from the static contribution, the total BBR shift also includes a dynamic contribution, which is derived from the combination of theoretical calculations and measurements of the $^3D_1$ state lifetime [5,16]. Reference [17] estimated the dynamic contribution in Mg to be 0.1% for the $^3P_0$ state, remarkably smaller than those of Yb (1%) and Sr (4%).

For bosonic atoms, optical dipole excitation of the electronic ground state $^1S_0$ to $^3P_0$ is strongly suppressed. A magnetic field enhances the dipole coupling, enabling a nanohertz linewidth by mixing the $^3P_1$ electronic state [12,18]. References [12,19] calculated the associated second-order Zeeman effect for Mg to be $-217(11)$ MHz/T^2 [equivalent to a fractional frequency shift of $-3.31(17) \times 10^{-7}$/T^2], a systematic effect that must be evaluated. We precisely measure the magnetic field dependence, which is consistent within the uncertainty of Ref. [12], estimated to be 5% [19]. This second-order Zeeman shift is larger than those of Yb [$-6.6(4)$ MHz/T^2 or $-1.27(8) \times 10^{-8}$/T^2 [18]] and Sr [$-23.5(2)$ MHz/T^2 or $-5.47(47) \times 10^{-8}$/T^2 [20]].

In this way, we directly measure the transition frequency, which agrees with the difference of the measured frequencies of the $^1S_0$-$^3P_1$ and $^3P_0$-$^3P_1$ transitions [7,8]. Because of its low mass and the short magic wavelength, Mg has a large photon recoil frequency shift $\Delta\nu_R = h/2\lambda^2_{\mathrm{magic}}m_{\mathrm{Mg}}$, where λ_{magic} is the magic wavelength, as well as greater tunneling. A deeper lattice is therefore required to suppress tunneling [21], as compared to heavier species.

We briefly summarize the steps required for the optical lattice spectroscopy in Fig. 1. A thermal beam of Mg atoms is slowed and loaded into a "singlet"-magneto-optical trap (MOT) using laser light tuned near the $^1S_0$-$^1P_1$

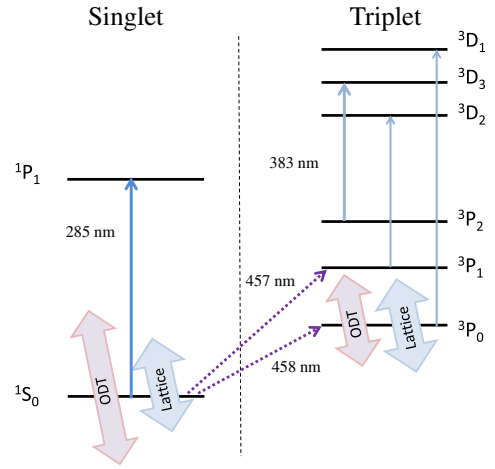

FIG. 1 (color online). Optical transitions in ^{24}Mg relevant for optical lattice spectroscopy. Atoms are continuously loaded into the long-lived electronic state $^3P_0$ in an optical dipole trap (ODT) at 1064 nm using a dual MOT [23]. Atoms trapped in a MOT using the $^1S_0$-$^1P_1$ transition are optically transferred with 457 nm light to the $^3P_1$ state and then to $^3P_2$. The atoms are further cooled in a MOT with 383 nm light that excites the ^3D manifold, and cold atoms are permitted to accumulate in $^3P_0$ in the ODT. These atoms are optically depumped to the ground state via $^3P_1$, and the magic-wavelength optical lattice is adiabatically turned on. The dipole trap and the optical lattice laser beams are depicted by the bold arrows. The 458 nm light interrogates the magnetic-field-enhanced clock transition.

transition. Atoms are optically transferred, after excitation to the $^3P_1$ state, into a second, simultaneously operated "triplet" $^3P_2$-$^3D_3$ MOT. There, atoms can decay to the $^3P_1$ state (see Fig. 1) during MOT operation [22] and have to be recycled with light exciting them to the $^3D_2$ state. This continuous loading scheme yields nearly 10^5 atoms in the $^3P_0$ state within 1 s at 100 μK in a 1064 nm dipole trap as in Ref. [23]. The atoms are then optically pumped to the $^3D_2$ state for 360 ms and decay to the electronic ground state via the $^3P_1$ state. Afterwards, a spatially overlapped 1D optical lattice with a waist of 89 μm is adiabatically turned on in 100 ms before the dipole trap is rapidly switched off. To select the coldest atoms, the optical lattice intensity is ramped to a lower depth and subsequently increased to a final value for the clock transition spectroscopy. Each of these linear intensity variations is performed within 100 ms. This procedure reproducibly generates about 1000 atoms at 4 μK.

We generate 160 mW of lattice light near the magic wavelength at $\lambda_{\text{magic}} = 469$ nm with a frequency-doubled Ti:sapphire laser. A horizontal buildup cavity, with a finesse of 80, twines around the vacuum chamber and, with a circulating power of ~2.3 W, produces trap depths of ten recoil energies $h\nu_R$. The cavity length is stabilized to the frequency of the laser with a Pound-Drever-Hall [24] lock driving an electro-optical modulator and a piezo-controlled mirror. An additional feedback loop driving an acousto-optical modulator (AOM) can set and stabilize the depth of the lattice. The light transmitted through the cavity is used to measure the circulating light intensity in the cavity.

The clock transition spectroscopy is performed with a homebuilt external cavity diode laser stabilized to an ultrastable resonator with finesse $\mathcal{F} = 600000$ at 916 nm, similar to Ref. [25]. The infrared light is fiber guided to the spectroscopy setup, a tapered amplifier chip, and a commercial second-harmonic generation stage. The system generates 10 mW of 458 nm light with a short-term frequency instability as low as 5×10^{-16} in 1 s, inferred with the help of a second ultrastable resonator. The spectroscopy is performed by irradiating the atoms for 100 ms with a pulsed, Gaussian-shaped laser beam with a waist of 300 μm and a peak intensity of 7 W/cm^2. The MOT coils, operated in a Helmholtz configuration, generate a magnetic field of 2.49(1) G/A, determined via optical Zeeman spectroscopy of the $^1S_0(m_J = 0)$-$^3P_1(m_J = \pm 1)$ transitions, increasing the dipole coupling of $^1S_0$ and $^3P_0$. We normally use a magnetic field of 249 G, which yields a predicted linewidth of 8.07 μHz and a Rabi frequency of 205 Hz [12]. In this way, we resonantly excite up to 1000 atoms to $^3P_0$, which are then optically pumped to $^3P_2$ and detected with 80 ms of fluorescence from the triplet MOT. This detection scheme yields a sensitivity of a few tens of atoms. To obtain the line center and profile of the transition, we record the number of excited atoms as we step the frequency of the 458 nm laser. The initial drift of the laser is determined via spectroscopy of the atoms and compensated with a feedforward of an AOM that shifts the laser frequency to a resonance of our ultrastable cavity. A scan over the resonance typically comprises 30 measurements, each lasting 1.9 s.

The magic wavelength for ^{24}Mg is inferred from measurements of the line center for different lattice depths and several wavelengths. Figure 2(a) shows two sets of measurements of the transition probability (red and blue dots) versus the clock laser frequency and corresponding Gaussian fits (red and blue solid curves) for three depths of a 466.97 nm lattice. The line profiles for different trap depths were measured successively. To evaluate and correct the residual laser drift, the measurement sequence was repeated three times, and the shift of the line centers for a specific trap depth is determined from the Gaussian fits. From the frequencies for a specific lattice depth, we infer the residual clock laser drift, which can be as large as 2–3 kHz within several minutes. The line profiles in Fig. 2(a) are three superposed scans. The linewidth of each profile, on the order of a few kilohertz, is mostly due to tunneling in our shallow optical lattice. According to Ref. [21], the total line broadening is on the order of twice the ground state bandwidth, in agreement with our findings. In our current apparatus, the trap depth was as low as six recoil energies, which gives rise to a carrier width of

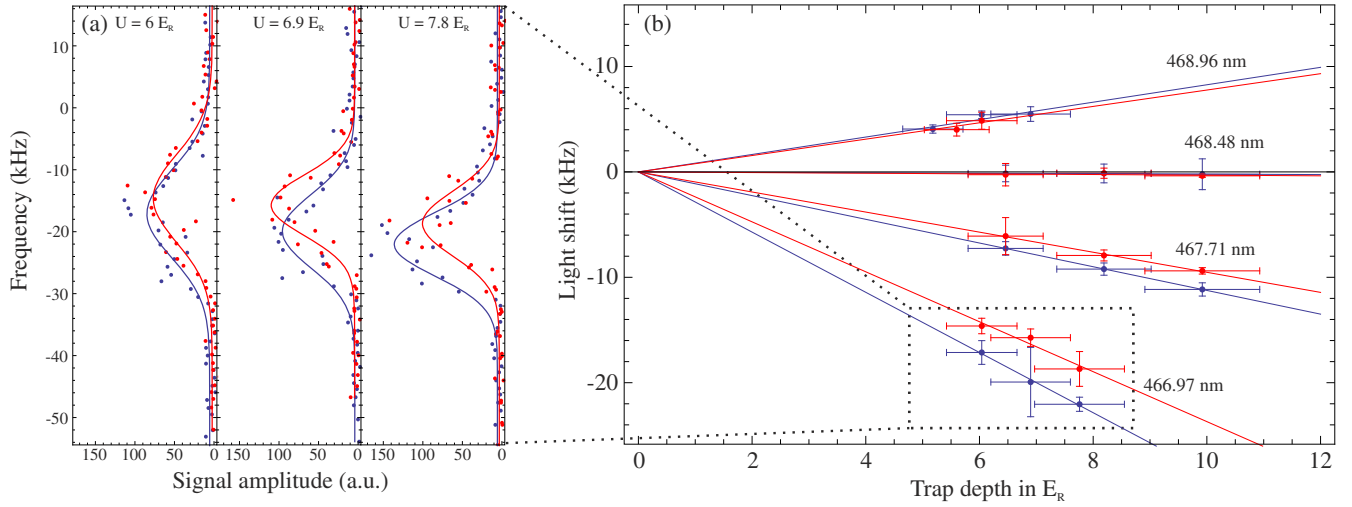

FIG. 2 (color online). (a) Measured and fit line profiles for three depths of a 466.97 nm optical lattice. Two sets of measurements (red and blue dots) are shown with their corresponding Gaussian fits (red and blue solid lines). (b) The observed linear ac Stark shift versus the optical lattice depth for several lattice wavelengths. The frequencies of the line center (dots) from Gaussian fits as in (a) and their corresponding linear regression (solid lines) are depicted. For each measurement set at a lattice wavelength, a single frequency offset accounts for the drift of our ultrastable cavity.

approximately 16 kHz. Figure 2(b) shows the line centers (dots) and the corresponding linear regression (solid lines) of the ac Stark shifts versus the lattice depth for different lattice wavelengths. An offset frequency was subtracted from the linear regressions for each lattice wavelength to account for the laser drift between measurements. The uncertainty of the experimental determination of the lattice depth is about 5% dominated by the uncertainty of the lattice waist. The uncertainty of the ac Stark shift is a combination of the statistical uncertainty of the linear regression and the systematic uncertainty of residual (nonlinear) frequency drifts of the clock laser, on the order of a few kilohertz. During the measurements for 466.97 nm, the clock laser was less stable, leading to more noise in the number of detected atoms, larger error bars, and a larger variation of the observed ac Stark shifts. The differences in the linear regression from the two measurement campaigns agree within these uncertainties. Separately, the two data sets yield magic wavelengths of 468.47(22) (blue data) and 468.45(19) nm (red data). Applying a linear regression to the combination of both measurement sets, we determine the magic wavelength of the ^{24}Mg $^1S_0$-$^3P_0$ transition to be 468.46(21) nm and the linear ac Stark shift dependence on the lattice depth and wavelength to be $1.67(12)\ \mathrm{kHz}/E_R/\mathrm{nm}$ [equivalent to a fractional frequency shift of $2.55(18) \times 10^{-12}/E_R/\mathrm{nm}$].

The experimentally determined magic wavelength agrees well with our theoretical prediction. We use a state-of-the-art relativistic approach that combines configuration interaction and all-order linearized coupled-cluster methods (CI + all-order). To evaluate the uncertainty of our calculations, we use a combination of the CI and second-order many-body perturbation theory (CI + MBPT), which does not include all-order corrections to the effective Hamiltonian. The difference of the CI + MBPT and CI + all-order values serves as an estimate of the theoretical accuracy [26–28]. The results are summarized in Table I. Our final recommended value for the theoretical Mg magic wavelength, listed in the "Final" row, uses measured instead of calculated transition energies for the dominant contributions. While our calculated Mg transition

TABLE I. Comparison of CI + MBPT and CI + all-order values for magic wavelengths λ_{magic} in nanometers and static polarizabilities α (in atomic units) of Mg, Sr [28], and Yb [27]. $\Delta\alpha = \alpha(nsnp\,^3P_0) - \alpha(ns^2\,^1S_0)$. The "Final" value in the third line uses measured instead of calculated energies of the most important polarizability contributions in the CI + all-order calculation.

Quantity	Method	Mg	Sr	Yb
λ_{magic}	CI + MBPT	468.45	847	789
	CI+all	468.68	820	754
	Final	468.45(23)		
	Exp.	468.46(21)	813.427[a]	759.354[a]
$\alpha(^1S_0)$	CI + MBPT	71.257	195.4	138.3
	CI + all	71.251	197.8	140.9
$\alpha(^3P_0)$	CI + MBPT	100.812	482.1	305.9
	CI + all	100.922	458.1	293.2
$\Delta\alpha$	CI + all	29.671	260.3[b]	152.3
	Exp.		247.379(7)	145.726(3)

[a]We only list six significant figures from the measurements in Refs. [29,30].
[b]Using experimental energies gives 254.4 a.u., and small corrections yield 247.5 a.u.

energies agree with the observed values to a few cm^{-1}, even these small differences affect the magic wavelength in the fourth significant figure. We note that this correction is quite small and the final value differs from the *ab initio* CI + all-order value by only 0.05%.

In Table I, we give CI + MBPT and CI + all-order values for the magic wavelength λ_{magic}. We also give the static ground state $\alpha(ns^2\,{}^1S_0)$ and excited clock state $\alpha(nsnp\,{}^3P_0)$ polarizabilities and their difference $\Delta\alpha$, which is proportional to the static BBR shift [17]. To demonstrate the extremely high accuracy of the theoretical calculations in Mg, we compare the magic wavelength and polarizabilities of Mg, Sr, and Yb in Table I. In our theoretical method, the main difference between Mg, Sr, and Yb are the much larger and more complicated cores of Sr and Yb than of Mg. As a result, core-valence correlations are much smaller in Mg than in Sr and Yb, leading to substantially higher accuracy for the theoretical predictions for Mg. The large differences between CI + MBPT and CI + all-order Sr and Yb values illustrate the significance of higher-order effects in these heavier systems. We note that the difference of the CI + MBPT and CI + all-order values for Sr and Yb is much larger than the difference of the CI + all-order results with experiment for both the magic wavelength and $\Delta\alpha$, confirming the validity of using such a difference as an uncertainty estimate of the Mg theoretical values. The excellent agreement of the CI + MBPT and CI + all-order polarizabilities indicates an uncertainty of the Mg BBR shift of less than 1%.

The second-order Zeeman shift drops out of the determination of the magic wavelength but is a significant correction to our measured transition frequency. Figure 3 shows the measured transition frequency versus the applied magnetic field (squares), a parabolic fit (black curve) of the measurements, and a theoretical prediction by Ref. [12] (red curve). The experimental parabolic coefficient is $-206.6(2.0)$ MHz/T^2 [equivalent to $-3.15(3)\times10^{-7}$/T^2] and agrees within 5% with a theoretical value, which is consistent with its estimated uncertainty [19]. The measurement accuracy of the magnetic field strength, via the Zeeman spectroscopy of the ${}^1S_0$-${}^3P_0$ transition, is 1% and limited by our present accuracy in measuring the MOT coils' electrical current.

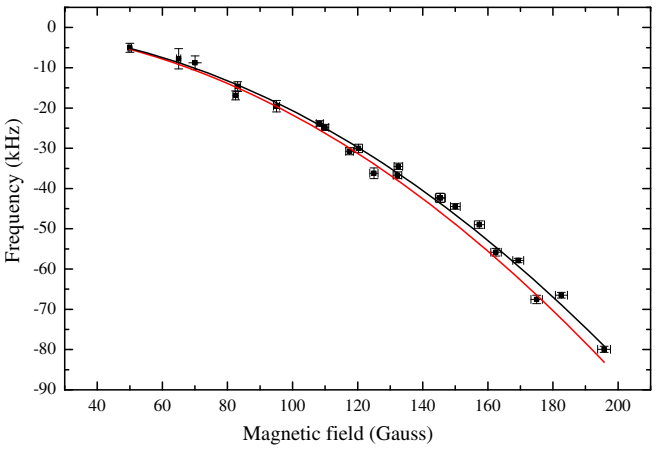

FIG. 3 (color online). Quadratic Zeeman shift of the clock transition versus magnetic field strength (black squares), a parabolic fit (black curve), and the theoretical prediction of Ref. [12] (red curve). The predicted dependence on the magnetic field is $-217(11)$ MHz/T^2, which agrees with the experimental result of $-206.6(2.0)$ MHz/T^2.

Our measurements at the magic wavelength, with the correction of the second-order Zeeman shift, yield a direct measurement of the optical transition frequency of 655 058 646 691(101) kHz. The absolute frequency is measured by beating the spectroscopy laser with an optical frequency comb that is stabilized to a 10 MHz GPS frequency reference. The measured transition frequency agrees with the difference of previous spectroscopic measurements of the ${}^1S_0$-${}^3P_1$ and ${}^3P_0$-${}^3P_1$ transitions of 655 659 923 839 730(48) and 601 277 157 870.0(0.1) Hz to better than 100 kHz, which corresponds to the estimated uncertainty of this measurement [7,8].

In summary, we report the direct optical spectroscopy of the ${}^1S_0$-${}^3P_0$ clock transition of laser-cooled bosonic ^{24}Mg in a magic-wavelength optical lattice. Our measurements determine precisely the magic wavelength and confirm the high precision obtained with a new theoretical atomic model of Mg. Our experimental determination of the quadratic Zeeman effect and clock transition frequency agree with a prediction [12] and previous indirect frequency measurements. Lattices with a larger depth of more than 40 recoil energies, accessible with higher laser power and a higher finesse of the enhancement cavity, will display a reduced width of the lowest vibrational band to 20 Hz and thus allow more precise spectroscopic measurements.

The demonstrated agreement of our combination of theory and experimental measurements is an important ingredient for exploring a future bosonic and fermionic Mg optical lattice clock. For bosonic magnesium, atoms can be optically prepared at microkelvin temperatures, which has not yet been demonstrated for the fermionic isotope ^{25}Mg. In our experiment, a dilute atomic cloud of 1000 atoms is distributed over 130 000 lattice sites ($\sim$0.008 atoms per lattice site), which is a factor of 100 lower density than that reported for other clocks with approximately the same number of atoms [31,32], significantly reducing the limitations from collisional shifts. The quadratic Zeeman shift can be sufficiently controlled [33] by using the suitably narrow Mg transitions for Zeeman spectroscopy, a higher clock laser intensity, and a smaller magnetic field [12]. A clock laser intensity of 7 W/cm^2 yields a Rabi frequency of 20 Hz, with a magnetic field that is 10 times smaller and a corresponding reduction in the uncertainty of the quadratic Zeeman shift. Here, in the context of Sr, Yb, and Hg, Mg can use higher clock laser intensities, because the clock and magic wavelengths are nearly equal, leading to small

differential polarizabilities of the Mg clock states and a naturally smaller clock-laser ac Stark shift. Combining all of these techniques can exploit the small Mg sensitivity to blackbody radiation to make a highly accurate and stable lattice clock and further precisely test atomic models for precision spectroscopy.

We thank A. Bauch and H. Schnatz from Physikalisch Technische Bundesanstalt (PTB) for providing a passive H maser and assistance with frequency measurements during the early stage of the experiment as well as C. Lisdat for helpful discussions. This work was supported in part by Deutsche Forschungsgemeinschaft (DFG) within QUEST, Center for Quantum Engineering and Space-Time Research (A. P. K., S. R., S. S., W. E., and E. M. R.), NASA (K. G.), and U.S. NSF Grants No. PHY-1404156 (M. S. S. and S. G. P.) and No. PHY-1311570 (K. G.). D. F. and K. H. Z. acknowledge financial support from DFG Research Training Group (Graduiertenkolleg) 1729. N. J. is supported by the Marie Curie Initial Training Network FACT (ITN-FACT) Program, call FP7-PEOPLE-2013-ITN.

[1] C. W. Chou, D. B. Hume, J. C. J. Koelemeij, D. J. Wineland, and T. Rosenband, Phys. Rev. Lett. **104**, 070802 (2010).
[2] N. Hinkley, J. A. Sherman, N. B. Phillips, M. Schioppo, N. D. Lemke, K. Beloy, M. Pizzocaro, C. W. Oates, and A. D. Ludlow, Science **341**, 1215 (2013).
[3] B. J. Bloom, T. L. Nicholson, J. R.Williams, S. L. Campbell, M. Bishof, X. Zhang, W. Zhang, S. L. Bromley, and J. Ye, Nature (London) **506**, 71 (2014).
[4] I. Ushijima, M. Takamoto, M. Das, T. Ohkubo, and H. Katori, Nat. Photonics **9**, 185 (2015).
[5] T. Nicholson, S. Campbell, R. Hutson, G. Marti, B. Bloom, R. McNally, W. Zhang, M. Barrett, M. Safronova, G. Strouse, W. Tew, and J. Ye, Nat. Commun. **6**, 6896 (2015).
[6] K. Beloy, N. Hinkley, N. B. Phillips, J. A. Sherman, M. Schioppo, J. Lehman, A. Feldman, L. M. Hanssen, C. W. Oates, and A. D. Ludlow, Phys. Rev. Lett. **113**, 260801 (2014).
[7] A. Godone and C. Novero, Metrologia **30**, 163 (1993).
[8] J. Friebe, M. Riedmann, T. Wübbena, A. Pape, H. Kelkar, W. Ertmer, U. Sterr, S. Weyers, G. Grosche, H. Schnatz, and E. M. Rasel, New J. Phys. **13**, 125010 (2011).
[9] R. Santra, K. V. Christ, and C. H. Greene, Phys. Rev. A **69**, 042510 (2004).
[10] V. D. Ovsyannikov, V. G. Pal'chikov, H. Katori, and M. Takamoto, Quantum Electron. **36**, 3 (2006).
[11] A. Derevianko, B. Obreshkov, and V. A. Dzuba, Phys. Rev. Lett. **103**, 133201 (2009).
[12] A. V. Taichenachev, V. I. Yudin, C. W. Oates, C. W. Hoyt, Z. W. Barber, and L. Hollberg, Phys. Rev. Lett. **96**, 083001 (2006).
[13] J. Mitroy, M. S. Safronova, and C. W. Clark, J. Phys. B **43**, 202001 (2010).
[14] T. Middelmann, S. Falke, C. Lisdat, and U. Sterr, Phys. Rev. Lett. **109**, 263004 (2012).
[15] J. A. Sherman, N. D. Lemke, N. Hinkley, M. Pizzocaro, R. W. Fox, A. D. Ludlow, and C. W. Oates, Phys. Rev. Lett. **108**, 153002 (2012).
[16] K. Beloy, J. A. Sherman, N. D. Lemke, N. Hinkley, C. W. Oates, and A. D. Ludlow, Phys. Rev. A **86**, 051404 (2012).
[17] S. G. Porsev and A. Derevianko, Phys. Rev. A **74**, 020502 (R) (2006); **86**, 029904(E) (2012).
[18] Z. W. Barber, C. W. Hoyt, C. W. Oates, L. Hollberg, A. V. Taichenachev, and V. I. Yudin, Phys. Rev. Lett. **96**, 083002 (2006).
[19] A. V. Taichenachev (private communication).
[20] P. G. Westergaard, J. Lodewyck, L. Lorini, A. Lecallier, E. A. Burt, M. Zawada, J. Millo, and P. Lemonde, Phys. Rev. Lett. **106**, 210801 (2011).
[21] P. Lemonde and P. Wolf, Phys. Rev. A **72**, 033409 (2005).
[22] P. L. Hansen, K. T. Therkildsen, N. Malossi, B. B. Jensen, E. D. van Ooijen, A. Brusch, J. H. Müller, J. Hald, and J. W. Thomsen, Phys. Rev. A **77**, 062502 (2008).
[23] M. Riedmann, H. Kelkar, T. Wübbena, A. Pape, A. Kulosa, K. Zipfel, D. Fim, S. Rühmann, J. Friebe, W. Ertmer, and E. Rasel, Phys. Rev. A **86**, 043416 (2012).
[24] R. W. P. Drever, J. L. Hall, F. V. Kowalski, J. Hough, G. M. Ford, A. J. Munley, and H. Ward, Appl. Phys. B **31**, 97 (1983).
[25] A. Pape, O. Terra, J. Friebe, M. Riedmann, T. Wübbena, E. M. Rasel, K. Predehl, T. Legero, B. Lipphardt, H. Schnatz, and G. Grosche, Opt. Express **18**, 21477 (2010).
[26] M. S. Safronova, M. G. Kozlov, and C. W. Clark, Phys. Rev. Lett. **107**, 143006 (2011).
[27] M. S. Safronova, S. G. Porsev, and C. W. Clark, Phys. Rev. Lett. **109**, 230802 (2012).
[28] M. S. Safronova, S. G. Porsev, U. I. Safronova, M. G. Kozlov, and C. W. Clark, Phys. Rev. A **87**, 012509 (2013).
[29] A. D. Ludlow *et al.*, Science **319**, 1805 (2008).
[30] Z. W. Barber, J. E. Stalnaker, N. D. Lemke, N. Poli, C. W. Oates, T. M. Fortier, S. A. Diddams, L. Hollberg, C. W. Hoyt, A. V. Taichenachev, and V. I. Yudin, Phys. Rev. Lett. **100**, 103002 (2008).
[31] A. D. Ludlow, N. D. Lemke, J. A. Sherman, C. W. Oates, G. Quéméner, J. von Stecher, and A. M. Rey, Phys. Rev. A **84**, 052724 (2011).
[32] S. Falke, N. Lemke, C. Grebing, B. Lipphardt, S. Weyers, V. Gerginov, N. Huntemann, C. Hagemann, A. Al-Masoudi, S. Häfner, S. Vogt, U. Sterr, and C. Lisdat, New J. Phys. **16**, 073023 (2014).
[33] Other clock spectroscopy schemes can suppress it, as has been explored in Refs. [34–36].
[34] V. I. Yudin, A. V. Taichenachev, C. W. Oates, Z. W. Barber, N. D. Lemke, A. D. Ludlow, U. Sterr, C. Lisdat, and F. Riehle, Phys. Rev. A **82**, 011804(R) (2010).
[35] T. Zanon-Willette, S. Almonacil, E. de Clercq, A. D. Ludlow, and E. Arimondo, Phys. Rev. A **90**, 053427 (2014).
[36] N. Huntemann, B. Lipphardt, M. Okhapkin, C. Tamm, E. Peik, A. V. Taichenachev, and V. I. Yudin, Phys. Rev. Lett. **109**, 213002 (2012).